

Tail-assisted pitch control in lizards, robots and dinosaurs

Thomas Libby¹, Talia Y. Moore², Evan Chang-Siu³, Deborah Li², Daniel J. Cohen⁴, Ardian Jusufi² & Robert J. Full²

In 1969, a palaeontologist proposed¹ that theropod dinosaurs used their tails as dynamic stabilizers during rapid or irregular movements, contributing to their depiction as active and agile predators. Since then the inertia of swinging appendages has been implicated in stabilizing human walking^{2,3}, aiding acrobatic manoeuvres by primates^{4–8} and rodents⁹, and enabling cats to balance on branches¹⁰. Recent studies on geckos^{11–13} suggest that active tail stabilization occurs during climbing, righting and gliding. By contrast, studies on the effect of lizard tail loss show evidence of a decrease, an increase or no change in performance^{14,15}. Application of a control-theoretic framework could advance our general understanding of inertial appendage use in locomotion. Here we report that lizards control the swing of their tails in a measured manner to redirect angular momentum from their bodies to their tails, stabilizing body attitude in the sagittal plane. We video-recorded Red-Headed Agama lizards (*Agama agama*) leaping towards a vertical surface by first vaulting onto an obstacle with variable traction to induce a range of perturbations in body angular momentum. To examine a known controlled tail response, we built a lizard-sized robot with an active tail that used sensory feedback to stabilize pitch as it drove off a ramp. Our dynamics model revealed that a body swinging its tail experienced less rotation than a body with a rigid tail, a passively compliant tail or no tail. To compare a range of tails, we calculated tail effectiveness as the amount of tailless body rotation a tail could stabilize. A model *Velociraptor mongoliensis* supported the initial tail stabilization hypothesis¹, showing as it did a greater tail effectiveness than the Agama lizards. Leaping lizards show that inertial control of body attitude can advance our understanding of appendage evolution and provide biological inspiration for the next generation of manoeuvrable search-and-rescue robots.

Agama lizards (average mass, 66.96 ± 2.93 g) ran within an acrylic track and rapidly transitional to a vertical wall with a shelter on top. To simulate a leap with a long aerial phase, we directed the animals over a small box that acted as a vault (Fig. 1a, b). To induce perturbations during the transition, we varied the traction available on top of the vault. We proposed that a sandpaper-covered vault would allow the lizard sufficient traction to closely direct its ground reaction force vector through its centre of mass (COM) and thereby minimize body rotation in the aerial phase (Fig. 1a and Supplementary Movie 1). Covering the vault with smooth card stock (Fig. 1b and Supplementary Movie 2) would cause feet to slip, misaligning the ground reaction force vector and imparting a rotational impulse during this critical phase when lizards redirect horizontal momentum upwards. We recorded body and tail motion with a high-speed digital camera.

To quantify the possible effect a tail has on maintaining attitude stability in the pitch axis during the leap, we determined the angle through which a tailless body would rotate after a given perturbation at take-off. We measured the perturbation magnitude at take-off for each trial by estimating the mean total angular momentum (H) over the duration of the leap. We computed H using the lizard's kinematic

data during the aerial phase by fitting a two-link (body and tail), planar dynamic model constructed from morphometric data from five Agama lizard cadavers (Supplementary Table 1). Assuming aerodynamic forces to be negligible^{8,12,13}, we took the computed H to be the perturbation applied during take-off. The variable surface vault produced a broad range in aerial-phase angular momentum, $\pm 1.5 \times 10^{-3} \text{ kg m}^2 \text{ s}^{-1}$. To better compare the magnitude of the perturbation among individuals, we normalized H by body moment of inertia (I_b) about its COM and by leap duration (t). The normalized perturbation magnitude, $(H/I_b)t$ (Fig. 2, abscissa), represents the angle through which an individual's body would rotate without its tail, given the observed angular momentum and trial duration. Because the duration of foot slippage was brief, take-off angle was not affected by the perturbation (coefficient of determination, $r^2 = 0.13$). Hence, we proposed that a constant body angle was maintained after the perturbation.

We reasoned that defining inertial appendage control over a range of perturbations could benefit from a physical model with a known control mechanism. We built an Agama-sized, tailed robot that used proportional-derivative (PD) feedback control (Fig. 1c, d) to stabilize body angle¹⁶. Inertial stabilization of robotic locomotion has been modelled before¹⁷, and simple air-righting accomplished¹⁸, but our robot is the first with a specialized tail-like appendage for continuous inertial stabilization. Previous investigations of tails in mobile robots have focused on substrate interaction and passive stability^{19,20}. Our wheeled robot swung an aluminium rod tail in the sagittal plane in response to sensing using a microelectromechanical systems gyroscope. A ski-jump-like ramp launched the robot at the same take-off angle that the lizards selected. The unbalanced gravitational moment as the front wheels left the ramp applied a similar rotational perturbation to that induced on the lizards by the low-friction vault. We launched the robot in two situations: with the controller off and the tail rigidly held parallel to the body (Fig. 1c and Supplementary Movie 3) and with the PD feedback controller on and the reference angle set to the take-off angle of the ramp (Fig. 1d and Supplementary Movie 4). Varying the perturbation on the robot by changing the speed with which it left the ramp altered the imparted angular momentum. As the perturbation increased, the robot with PD feedback tail control maintained a nearly constant body angle by swinging its tail upward and incurred 72% less rotation after a perturbation than did the robot without tail control (Fig. 2b).

Lizards swung their tails during leaps in a manner consistent with the control of body pitch observed in the robot. Tail swinging was not an all-or-none behaviour, but was proportional to perturbation magnitude. The change in tail angle relative to the body during the aerial phase correlated with the normalized perturbation magnitude ($r = 0.79$, $P < 0.001$). A larger perturbation at take-off resulted in a correspondingly greater tail swing. Attenuation of body pitch was not unidirectional: lizards swung their tails upwards to compensate for nose-down perturbations and downwards in response to nose-up perturbations (Fig. 2a and Supplementary Movie 5). By rotating their

¹Center for Interdisciplinary Bio-Inspiration in Education and Research, University of California, Berkeley, California 94720-3140, USA. ²Department of Integrative Biology, University of California, Berkeley, California 94720-3140, USA. ³Department of Mechanical Engineering, University of California, Berkeley, California 94720-1740, USA. ⁴Department of Bioengineering, University of California, Berkeley, California 94720-1762, USA.

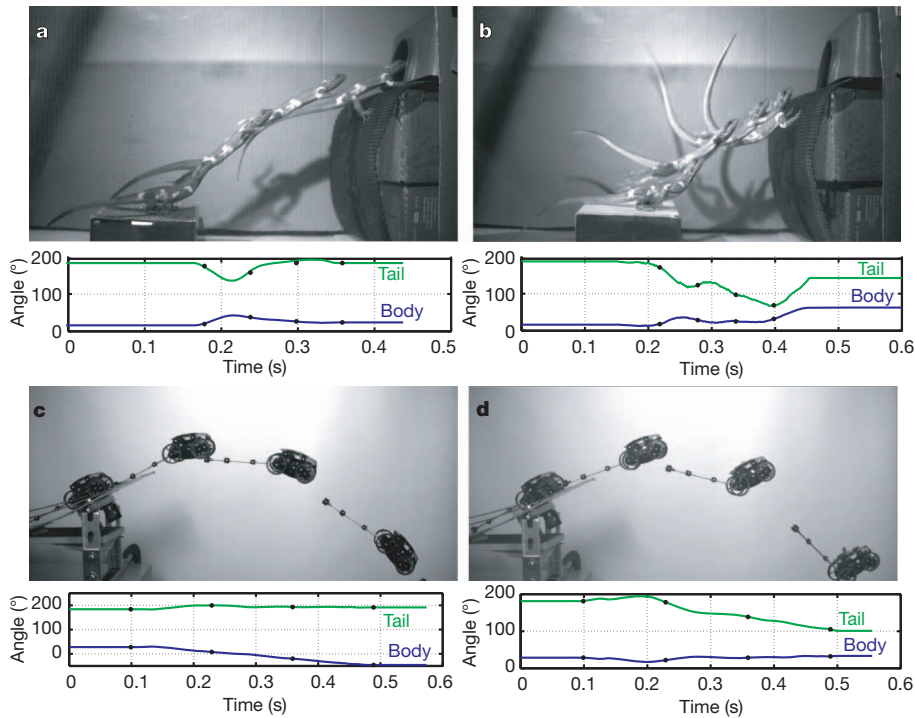


Figure 1 | Pitch stabilization using a tail in a lizard and robot. Tail angle (green) relative to body axis and body angle (blue) relative to ground. **a, b**, Agama lizards ran along a track and vaulted off an obstacle to a vertical wall with a shelter on top. Overlain images are separated by 60 ms. **a**, A high-traction vault surface produced small perturbations in body angular momentum, allowing tail and body angles to remain constant (Supplementary Movie 1). **b**, A low-traction vault surface produced slipping that generated an angular momentum perturbation. By swinging their tails upwards, lizards redirected

angular momentum from the body to the tail to maintain body angle (Supplementary Movie 2). **c, d**, A wheeled robot drove off a ramp, producing a nose-down perturbation in body angular momentum. Overlain images are separated by 130 ms. **c**, Without PD feedback control, the robot body and tail rotated as a rigid body (Supplementary Movie 3). **d**, With PD feedback control, the tail swung upwards as the controller applied torque to stabilize the body, keeping the body angle constant (Supplementary Movie 4).

tails with respect to the body in the sagittal plane, the lizards transferred angular momentum from the body to tail, thereby reducing body angular velocity and the effect of perturbation on body rotation (Fig. 2a).

We characterized the sensitivity to pitch perturbations by regressing experimentally observed rotations against the normalized perturbation,

yielding a dimensionless metric (S , the slope of the lines in Fig. 2a) representing the observed body rotation due to a perturbation relative to the rotation a tailless body would undergo. A sensitivity value, or slope, of one would indicate that the individual stabilized itself no better than would a tailless body. A value less than one signifies that the animal or robot attenuated the effect of the perturbation on its body rotation. A

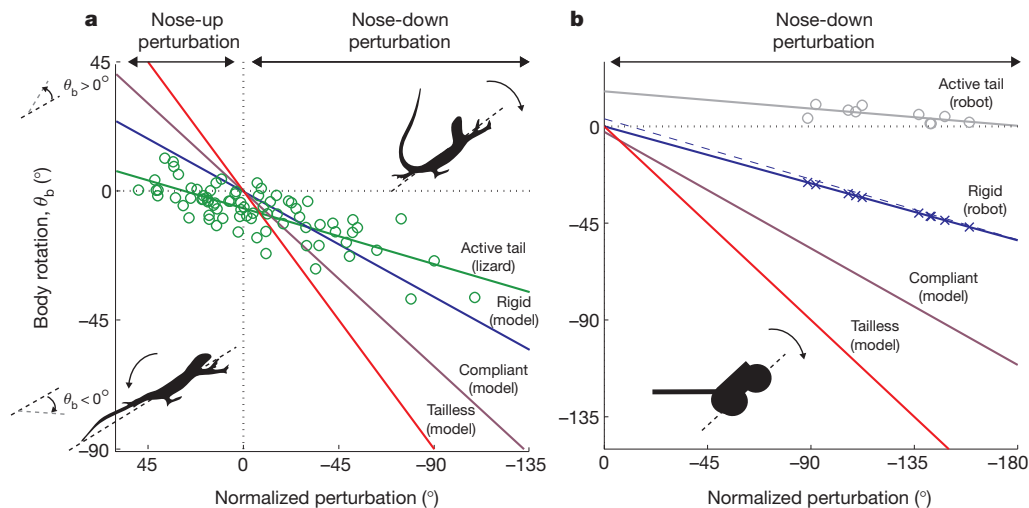


Figure 2 | Sensitivity of body rotation to a perturbation in a lizard and robot. Body rotation (θ_b) as a function of perturbation, defined as the angle through which the body would rotate without a tail. The slope of the lines represents sensitivity to perturbations. **a**, Lizards (green circles and line) controlled body rotation by swinging their tails downwards to correct a nose-up pitch (normalized perturbation, $>0^\circ$) and upwards to correct a nose-down pitch (normalized perturbation, $<0^\circ$). Lizards were less sensitive to

perturbations than were tailless (red), compliant-tail (purple) or rigid-tail (blue) Agama models. **b**, Robots (grey circles and line) controlled body rotation by swinging their tails upwards to correct a nose-down pitch (normalized perturbation, $<0^\circ$) more effectively than lizards. Robots were far less sensitive to perturbations than were tailless (red) and compliant-tail (purple) models or robots with rigid tails (blue crosses and line).

value of zero shows perfect compensation (Fig. 2a, b, horizontal dashed line). Supporting the hypothesis of tail-facilitated control, we found the measured sensitivity of Agama lizards to a rotational perturbation to be very low, $S = 0.22 \pm 0.02$, relative to the tailless model value, $S = 1$, although not as low as that of our PD-feedback-controlled tailed robot ($S = 0.090 \pm 0.035$; Supplementary Table 2).

We compared the lizard's effectiveness in controlling body pitch using an active tail with those of our robot and three mathematical models: a tailless animal (single body link), a rigid-tailed animal (body and tail links with a rigid joint), and a compliant tailed animal (both links with a torque-free pin joint). We used a morphologically averaged Agama model to generate a prediction of perturbation sensitivity for each passive tail condition, and calculated the difference with respect to the experimentally measured value (Supplementary Table 2). Adding a compliant or rigid tail to the tailless model Agama decreased its sensitivity by 36% ($S = 0.64$) or 58% ($S = 0.42$), respectively, indicating that passive tails can improve aerial stability. The actual Agamas actively controlling their tails were significantly less sensitive to perturbations than either passive tail model ($P < 0.001$; Supplementary Table 2). Our model results showed that animals received 48% less rotation after a perturbation than they would if they had held their tails rigid during the aerial phase, 66% less rotation than if they had left the tail compliant and 78% less rotation than if they had no tail at all. By comparing the average proportion of angular momentum in each segment with the expected value for a rigidly linked model, we found that the lizards had $41.000 \pm 0.043\%$ less angular momentum in their bodies than the rigid model, and a corresponding increase in tail momentum, indicating active momentum transfer.

The PD-feedback-controlled robot incurred 72% less rotation after a perturbation than it would if it had held its tail rigid during the aerial phase, 85% less rotation than if it had left the tail compliant and 91% less rotation than if it had no tail at all (Supplementary Table 2). The experimental control (that is, with PD feedback controller off) was not significantly different from the model case in which the tail was rigidly connected to the body (Fig. 2b, blue line and crosses; $t = -5.0$, $P < 0.001$). We found that the tail contained $31.00 \pm 0.04\%$ more angular momentum than if it was rotating rigidly with the body, and that the body contained $40.00 \pm 0.08\%$ less. With the PD feedback controller off, the passive-tail robot's links did not contain significantly different momentum than did the rigid model (analysis of variance, $F = 0.32$, $P = 0.58$). Hence, the effect of the PD feedback controller on regulating body angle was to redirect angular momentum from the body to the tail, supporting our hypotheses for lizards.

Our mathematical model allows us to predict the effectiveness of different tails in preventing body rotation. Assuming that total angular momentum is conserved after a perturbation, the tail must rotate for the body's orientation to remain stable. The amount of rotation required depends on tail morphology^{12,13}. We define tail effectiveness as the amount of tailless body rotation a tail could stabilize per degree of tail rotation (that is, the absolute value of the reciprocal slope from Fig. 3 linearized around a tail rotation of $\phi_t = 0^\circ$). For a tail effectiveness of one, a perturbation rotating a tailless animal by 45° could be completely stabilized by rotating the tail through the same angle. Less effective tails would require more tail rotation to stabilize the same perturbation. Because tails are limited in range of motion, effectiveness limits the size of perturbation a tail can completely stabilize. After modelling each lizard in our study, we found their average tail effectiveness to be 0.79: for the typical maximum tail stroke of 100° , the lizards could completely stabilize a perturbation that would rotate a tailless lizard by almost 80° (Fig. 3; range shown by green shaded area). When our robot's body-tail length ratio was similar to those of the Agama lizards, it was over twice as effective (1.84; Fig. 3, dashed line, bottom grey shaded area). This resulted from concentrating mass at the tip (Supplementary Table 1), rather than at the base as in lizards. We modelled a range of possible tail configurations in the robot, from a small tail (5% body mass, 50% body length) to a large tail (10%

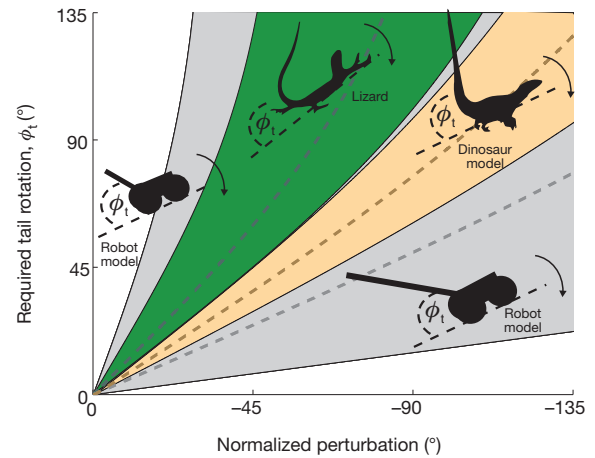


Figure 3 | Tail effectiveness for *A. agama*, *V. mongoliensis* and a robot with tail. Tail rotation (ϕ_t) required to prevent body rotation as a function of perturbation, defined as the angle through which the body would rotate without a tail, normalized by the observed angular momentum and trial duration. The slope of the lines represents the reciprocal of effectiveness (shallower slopes correspond to more effective tails). The average effectiveness for the Agama lizards was 0.79 (dashed line in green shaded area, which represents individual variation). Our robot had a more effective tail (black dashed line in lower grey shaded area), counteracting 1.84° of body rotation for each degree of tail rotation. A robot model with a tail 50% of the body length and 5% of the body mass was least effective (upper bound of grey shaded area), whereas a tail 200% of body length and 10% of the body mass was greater than three times more effective (lower bound of grey shaded area) than our robot. The *Velociraptor* model had a more effective tail than the most effective Agama lizard (slope, 1.23; dashed line in tan area, which represents 15% variation in model body and tail moment of inertia).

body mass, 200% body length). The smallest-tail model was far less effective than in lizards (Fig. 3, upper bound of grey area), whereas the largest-tail model (Fig. 3, lower bound of grey shaded area) was considerably more effective than even our actual robot.

Finally, we tested the original tail stabilization hypothesis¹ with regard to tail use in theropods. By using our model with a conservative morphometric reconstruction²¹, we found that *Velociraptor mongoliensis*²², an agile, 20-kg, 1.5-m-tall biped, with a tail effectiveness of 1.23 (Fig. 3, tan shaded area) given sufficient muscular capacity, could have outperformed even the most tail-effective Agama lizard. Although the distal portion of dromeosaur tails was bony and possibly stiff³, the proximal tail base could bend by up to 90° (ref. 23). Such a range of motion would enable *Velociraptor* to sustain a perturbation that would rotate a tailless animal by 110° , or to adjust its body angle by up to 45° in an unperturbed leap. Despite previously proposed limitations of passive tails²⁴, small theropods like *Velociraptor* with active tails might have been capable of aerial acrobatics beyond even those displayed by present-day arboreal lizards^{11–13}.

METHODS SUMMARY

Dynamic models. For simple characterization of the underlying dynamics of tail-assisted manoeuvres, we derived a planar, two-link, rigid-body model. By taking the derivative of the total angular momentum of each link and solving for the model's orientation and velocities with respect to actuation torque, we obtained a set of nonlinear, coupled ordinary differential equations realized in state-space form. We initialized the model with links oriented 180° apart. We set angular velocity of the tail link to zero and that of the body link such that the total angular momentum was as desired. We averaged the morphometrics of all animals to create the Agama model used in simulations. Simulations using morphometric models of individual Agama lizards did not yield significantly different perturbation sensitivities from those of the averaged Agama model. We performed numerical simulations in MATLAB.

Kinematics. To estimate the angular momentum of the animal or robot from kinematics, we treated the body and tail as rigid bodies with a hinge at the base of the tail (1 cm posterior to the vent in lizards). We used video tracking software (Xcitex PROANALYST) to capture kinematics, and calculated positions and velocities of

COMs in MATLAB. We estimated H from the two-link, rigid-body model for each video frame and averaged over the leap.

Statistics. We used multiple regression analysis in MATLAB to compare sensitivities (linear fits) of the experimental data to model hypotheses (t -test of slope). Sensitivities of individual animals were not significantly different from one another (analysis of variance, $F = 2.1$, $P = 0.073$).

Velociraptor model. To model the tail stabilization performance of an extinct theropod, we estimated mass properties from a two-dimensional reconstruction (Supplementary Table 1). We represented the head, trunk and lung capacity as ellipsoids, the neck as an elliptical cylinder, the limbs as point masses, and the tail as a truncated cone by digitizing points on the dorsal and sagittal views of the reconstruction. Estimates of combined trunk–tail moment of inertia agreed well with ref. 25.

Full Methods and any associated references are available in the online version of the paper at www.nature.com/nature.

Received 11 August; accepted 10 November 2011.

Published online 4 January 2012.

- Ostrom, J. H. Osteology of *Deinonychus antirrhopus*, an unusual theropod from the Lower Cretaceous of Montana. *Bull. Peabody Mus. Nat. Hist. (Paris)* **30**, 68–80, 144 (1969).
- Pijnappels, M. *et al.* Armed against falls: the contribution of arm movements to balance recovery after tripping. *Exp. Brain Res.* **201**, 689–699 (2010).
- Roos, P. E. *et al.* The role of arm movement in early trip recovery in younger and older adults. *Gait Posture* **27**, 352–356 (2008).
- Dunbar, D. C. Aerial maneuvers of leaping lemurs: the physics of whole-body rotations while airborne. *Am. J. Primatol.* **16**, 291–303 (1988).
- Larson, S. G. & Stern, J. T. Maintenance of above-branch balance during primate arboreal quadrupedalism: coordinated use of forearm rotators and tail motion. *Am. J. Phys. Anthropol.* **129**, 71–81 (2006).
- Günther, M. M., Ishida, H., Kumakura, H. & Nakano, Y. The jump as a fast mode of locomotion in arboreal and terrestrial biotopes. *Z. Morphol. Anthropol.* **78**, 341–372 (1991).
- Demes, B. *et al.* Body size and leaping kinematics in Malagasy vertical clingers and leapers. *J. Hum. Evol.* **31**, 367–388 (1996).
- Peters, A. & Preuschoft, H. in *Biology of Tarsiers* (ed. Niemitz, C.) 227–255 (Fischer, 1984).
- Bartholomew, G. A. & Caswell, H. H. Locomotion in kangaroo rats and its adaptive significance. *J. Mamm.* **32**, 155–169 (1951).
- Walker, C. *et al.* Balance in the cat: role of the tail and effects of sacrocaudal transection. *Behav. Brain Res.* **91**, 41–47 (1998).
- Jusufi, A., Goldman, D. I., Revzen, S. & Full, R. J. Active tails enhance arboreal acrobatics in geckos. *Proc. Natl Acad. Sci. USA* **105**, 4215–4219 (2008).
- Jusufi, A., Kawano, D. T., Libby, T. & Full, R. J. Righting and turning in mid-air using appendage inertia: reptile tails, analytical models and bio-inspired robots. *Bioinspir. Biomim.* **5**, 045001 (2010).
- Jusufi, A., Zeng, Y., Full, R. J. & Dudley, R. Aerial righting reflexes in flightless animals. *Integr. Comp. Biol.* **51**, 937–943 (2011).
- Bateman, P. W. & Fleming, P. A. To cut a long tail short: a review of lizard caudal autotomy studies carried out over the last 20 years. *J. Zool. (Lond.)* **277**, 1–14 (2009).
- Gillis, G. B., Bonvini, L. A. & Irschick, D. J. Losing stability: tail loss and jumping in the arboreal lizard *Anolis carolinensis*. *J. Exp. Biol.* **212**, 604–609 (2009).
- Chang-Siu, E., Libby, T., Tomizuka, M. & Full, R. J. in *IEEE/RSJ Internat. Conf. Intelligent Robots Systems 2011* 1887–1894 (IEEE, 2011).
- Berkemeier, M. D. & Fearing, R. S. Control of a two-link robot to achieve sliding and hopping gaits. *IEEE Trans. Robot. Autom.* **1**, 286–291 (1992).
- Mather, T. W. & Yim, M. in *IEEE/RSJ Internat. Conf. Intelligent Robots Systems 2009* 5905–5910 (IEEE, 2009).
- Hyun Soo, P. *et al.* in *IEEE Internat. Conf. Robotics Automation 2009* 2655–2660 (IEEE, 2009).
- Saunders, A. *et al.* The RiSE climbing robot: body and leg design. *Proc. SPIE* **6230**, 623017 (2006).
- Alexander, R. M. Dinosaur biomechanics. *Proc. R. Soc. B* **273**, 1849–1855 (2006).
- Paul, G. S. *The Princeton Field Guide to Dinosaurs* 137 (Princeton Univ. Press, 2010).
- Paul, G. S. *Dinosaurs of the Air: the Evolution and Loss of Flight in Dinosaurs and Birds* 45 (Johns Hopkins Univ. Press, 2002).
- Carrier, D. R. *et al.* Influence of rotational inertia on turning performance of theropod dinosaurs: clues from humans with increased rotational inertia. *J. Exp. Biol.* **204**, 3917–3926 (2001).
- Sellers, W. I. & Manning, P. L. Estimating dinosaur maximum running speeds using evolutionary robotics. *Proc. R. Soc. B* **274**, 2711–2716 (2007).

Supplementary Information is linked to the online version of the paper at www.nature.com/nature.

Acknowledgements We thank P. Jennings for video editing and figure production, T. Full for digitizing the lizard video and K. Padian for his advice on the dinosaur reconstruction and capability. We thank O. O'Reilly, S. Sponberg and N. Sapir for advice on analysis. This work was supported by a US NSF FIBR grant to R.J.F., a MAST CTA grant to R.J.F., an NSF IGERT under award DGE-0903711 and a Swiss NSF Fellowship to A.J.

Author Contributions T.L. designed the study and robot, carried out experiments, analysed data and wrote initial drafts of the manuscripts. T.Y.M. designed the study, carried out animal experiments and worked out kinematics. E.C.-S. designed and constructed the robot, carried out experiments and derived the analytical model. D.L. carried out experiments and worked out kinematics. D.J.C. designed experiments and collected and analysed animal kinematic data. A.J. designed and performed experiments and analysed data. R.J.F. directed the project, defined the analysis and wrote the final version of the manuscript.

Author Information Reprints and permissions information is available at www.nature.com/reprints. The authors declare no competing financial interests. Readers are welcome to comment on the online version of this article at www.nature.com/nature. Correspondence and requests for materials should be addressed to R.J.F. (rjfull@berkeley.edu).

METHODS

Animals. Wild-caught Red-Headed Agama lizards were purchased from a commercial vendor (<http://www.reptilescritters.com>). Six lizards (average mass, 66.96 ± 2.93 g; average snout-vent length, 12.75 ± 0.28 cm) were used for kinematic measurements. Lizards were housed in groups in large opaque tanks, kept in an environmentally controlled room ($25 \pm 2^\circ\text{C}$; relative humidity, 27%) with 12-h light-dark cycles and fed a diet of water and crickets. The Animal Care and Use Committee at the University of California, Berkeley, whose activities are mandated by the US Animal Welfare Act and Public Health Service Policy, approved all experimental procedures.

Experimental apparatus and protocol. We ran animals in a specially constructed track made of clear Lexan (acrylic) and steel (track dimensions: 150 cm (length), 30 cm (width), 40 cm (wall height)). The track was designed to allow the animals to reach top speed after an escape response. We placed a 22-cm-high wall at the end of the track; an enclosed plastic shelter at the top of the wall provided the target for the animals to complete the transition. We lined the exterior walls with tinted cellophane to limit the animal's field of view to the track interior.

In each trial, we placed the lizard at the beginning of the track and elicited an escape response by brushing the animal's tail. The animal accelerated rapidly into a run, made an intermediate jump onto the vault (dimensions, $24\text{ cm} \times 13\text{ cm} \times 6\text{ cm}$) and then jumped to the wall. The average horizontal speed during the aerial phase of the transition was $1.23 \pm 0.33\text{ m s}^{-1}$ (mean \pm s.d.). Animals transitioned using one of two general patterns. In 88% of trials, animals pitched up slightly and ran quadrupedally onto the box, where they reared onto their hind legs and jumped bipedally. In cases where their initial speed was high, animals initiated bipedal running before the vault and used the vault as a take-off platform with one or both legs. In all cases, contact with the vault was less than a stride, with contact from either one or both hind feet. Contact with the vault was critical to direct the jump upward to the wall. If animals attempted to jump over the vault they generally landed in the space between the vault and the wall. Hence, we were able to localize a critical transition area where animals must generate large ground reaction forces to initiate a jump. By reducing the traction on the vault, we could apply a perturbation during an important phase of the transition. We used either 60-grit sandpaper or smooth glossy card stock to vary friction on the top of the vault.

We defined a successful trial as one where the individual completed the vault to the wall without a pause. We excluded cases where the lizard struck the vault while climbing on to it, or slipped with one foot and gripped with the other, thereby applying a roll or yaw perturbation. In total, 77 trials from six individuals fitted our criteria for analysis. The selected trials comprised 34 leaps from the sandpaper and 43 leaps from the smooth substrate. Each individual was represented by at least eight trials in the data pool and all spanned a comparable range in perturbation magnitude.

We used topographical correction fluid to place markers on the head, torso, and tail for kinematic analysis. The track was lit with multiple lights and high-speed video was captured at 500 frames per second (X-PRI, AOS Technologies AG). We allowed animals to rest for 10–15 min between running bouts, and to recover for 90 min after every ten trials. The kinematics was extracted from videos with automated tracking software (ProAnalyst, Xcitex) and analysed in MATLAB (Mathworks).

Morphometrics. We used cadavers of five animals to construct a morphometric model of the animal. For both body and tail, we measured mass, distance from hip to segment COM, and moment of inertia (MOI) about COM (Supplementary Table 2). We used a pendulum technique to measure MOI, whereby the segment was deep-frozen and then supported by pins near the radius of gyration, following ref. 26. Two of the animals in the kinematic study subsequently died and were included in the morphometric study; the other three were from a previous study, but were in the same size range. We measured total body mass and snout-vent and tail-vent distances for the living animals. We used the average ratio of body mass to tail mass of the cadavers to estimate segment masses of the living animals. We estimated the MOI of the living animals by scaling the average MOI of cadavers by the product of segment mass and the square of segment length.

Kinematic analysis. We used a planar, two-link model to estimate the animal's total angular momentum during the aerial phase of the transition. We can write the angular momentum of the two-link model with respect to the system COM as

$$\mathbf{H}_o = I_b \boldsymbol{\omega}_b + m_b \boldsymbol{\rho}_b \times \dot{\boldsymbol{\rho}}_b + I_t \boldsymbol{\omega}_t + m_t \boldsymbol{\rho}_t \times \dot{\boldsymbol{\rho}}_t \quad (1)$$

where $\boldsymbol{\rho}_i$ is the vector from the animal's COM to the COM of the segment, $\boldsymbol{\omega}_i = \dot{\theta}_i \mathbf{E}_3$ is the angular velocity of the segment, $\dot{\theta}_i$ is the derivative of the segment angle, \mathbf{E}_3 is the vector orthogonal to the plane, I_i denotes the segment's MOI about its COM, m_i is the segment's mass, subscripts $i = b, t$ denote the body and tail, respectively, and the dot denotes the time derivative. The model did not capture additional angular momentum due to rotation of the limbs or bending of the body and hence represents a conservative estimate of the total perturbation applied.

We defined the position of the segments from the kinematic markers on the animal in each video frame during the aerial phase of the transition. Markers on the head, torso and tail were used to define the location of the body-link end point, the pin joint between the links, and the tail-link end point, respectively. We used our measurement of the segment COM position relative to the hip to calculate the instantaneous position of each segment in the model. The total COM was found by a mass-weighted average of the segment positions. From these vectors and their derivatives, along with measurements of MOI and mass, we calculated angular momentum for each segment at each frame using equation (1). Using the assumption of constant angular momentum, we took the magnitude of perturbation to be the mean measured angular momentum over the duration of the aerial transition.

Mathematical model. To test the hypothesis that perturbed animals manipulated angular momentum using their tails, we built a numerical dynamic model. Our task was simplified by the following experimental considerations. First, the critical period for stabilization (that is, maintenance of body pitch before landing) was spent entirely in the air, where only aerodynamic forces acted on the animal. These forces were found to be negligible in a somewhat smaller animal^{12,13} and we therefore ignored them here. Second, the perturbation was limited to the brief period directly before take-off. If no external forces acted on the animal, then total angular momentum was conserved. This allowed complete characterization of the perturbation impulse via measurement of the total angular momentum of the animal during the aerial phase. Finally, we restricted our analysis to rotations within the sagittal plane only. Trials that had out-of-plane perturbations were rejected. This allowed use of a relatively simple planar rigid-body model. We chose the simplest model possible: a two-link chain of rigid bodies, with one link representing the body and the other representing the tail.

The model was derived with the absolute body and tail angles referenced to horizontal as shown in Supplementary Fig. 1. We define a Cartesian coordinate system located at the COM of the system, resulting in the constraint $m_b \boldsymbol{\rho}_b + m_t \boldsymbol{\rho}_t = \mathbf{0}$. The two bodies are assumed to be joined by a pin joint, where the relative torque, $\tau = \tau \mathbf{E}_3$, represents actuation at the pivot. Assuming that no external forces act on the system during the manoeuvre, the time derivative of equation (1) is zero: $\dot{\mathbf{H}}_o = \mathbf{0}$. Hence, the derivative of the second link's angular momentum, $\dot{\mathbf{H}}_{t0}$, is easily written using the derivative of the first link's angular momentum, $\dot{\mathbf{H}}_{b0} = \tau + (\boldsymbol{\rho}_b - \boldsymbol{\rho}_t) \times m_b \dot{\boldsymbol{\rho}}_b$, where $\boldsymbol{\rho}_t$ is the vector from the pivot to the link COM. Solving for the states $\mathbf{x} = [\theta_b \quad \dot{\theta}_b \quad \theta_t \quad \dot{\theta}_t]^T$, yields a state-space model of the system in the form

$$\dot{\mathbf{x}} = \mathbf{f}(\mathbf{x}) + \mathbf{g}(\mathbf{x})u$$

where the states consist of the angular position and velocity of the links and the control input, $u = \tau$, is the relative torque. The details of $\mathbf{f}(\mathbf{x})$ and $\mathbf{g}(\mathbf{x})$ are as follows:

$$\mathbf{f}(\mathbf{x}) = \begin{bmatrix} \dot{\theta}_b \\ \frac{a\dot{\theta}_b^2 - b}{d - e} \\ \dot{\theta}_t \\ \frac{-a\dot{\theta}_t^2 + c}{d - e} \end{bmatrix} \quad \mathbf{g}(\mathbf{x}) = \begin{bmatrix} 0 \\ -\frac{f}{d - e} \\ 0 \\ \frac{g}{d - e} \end{bmatrix}$$

where

$$a = \frac{1}{2} I_b^2 I_t^2 m_b^2 m_t^2 \sin(2(\theta_b - \theta_t))$$

$$b = (I_t^2 m_b m_t + I_t(m_b + m_t)) l_b l_t m_b m_t \dot{\theta}_t^2 \sin(\theta_b - \theta_t)$$

$$c = (I_b^2 m_b m_t + I_b(m_b + m_t)) l_b l_t m_b m_t \dot{\theta}_b^2 \sin(\theta_b - \theta_t)$$

$$d = I_b^2 I_t^2 m_b^2 m_t^2 \cos(\theta_b - \theta_t)^2$$

$$e = (I_b^2 m_b m_t + I_b(m_b + m_t))(I_t^2 m_b m_t + I_t(m_b + m_t))$$

$$f = (I_t^2 m_b m_t + I_t(m_b + m_t)) \\ - l_b l_t m_b m_t \cos(\theta_b - \theta_t)(m_b + m_t)$$

$$g = (I_b^2 m_b m_t + I_b (m_b + m_t) - I_b I_t m_b m_t \cos(\theta_b - \theta_t))(m_b + m_t)$$

We used the model to calculate the sensitivity of lizards and robots with a compliant tail, and to estimate tail effectiveness in lizards, robots and *Velociraptor* (numerical solution in MATLAB using 'ode45').

Physical model (robot). To complement the mathematical model, we constructed a small bio-inspired robot to test the ability of an inertial appendage to stabilize aerial manoeuvres. We built our model by modifying a small commercial radio-controlled toy (RadioShack Flipz Truck). The design of the toy included two independent d.c. gear motors, which drove the left- and right-hand pairs of wheels. We modified the gear trains such that one gear motor drove the front wheels while the other drove a single pin joint at the rear, onto which we secured an aluminium rod (that is, a tail) approximately twice as long as the body. The tail was completed with the addition of a tunable mass at its distal end. Varying the mass at the tail tip allowed modulation of the tail's MOI. The resulting vehicle could move along a single axis (that is, it had no steering) and rapidly move its tail in the pitch-axis (that is, the sagittal plane of the robot).

We removed the toy's original electronics and installed a microcontroller (Arduino Pro Mini, Sparkfun Electronics), a single-axis microelectromechanical systems gyroscope (Invensense IDG-650) and a motor controller (Polulu TB6612FNG). The package was powered by small lithium-ion batteries (Turnigy 138mAh T1382S-10). This system enabled us to test the ability of simple feedback controllers to use a tail to stabilize body pitch orientation. Orientation of the vehicle was established by integrating the angular rate signal from the gyroscope. Because the accuracy of this scheme degrades with time, we limited the trials to 1–2 s. The controller was activated by a small button on the robot. After a 100-ms delay, the feedback controller ran for 2 s while logging angular velocity. We used a high-speed camera (X-PRI, AOS Technologies AG) to record kinematics at 1,000 frames per second.

We tested two common controllers: a proportional feedback controller and a PD feedback controller. Under the proportional controller, the motor torque was proportional to the difference between the current pitch (the integrated gyroscope measurement) and a desired orientation set at the beginning of the trial. The PD feedback control law added a torque proportional to the vehicle's pitch angular velocity (raw gyroscope signal). The controller had no knowledge of the angle or

velocity of the tail; the servomotors acted directly on the body angle. We tuned the controller gains and tail MOI by dropping the robot from a height of about 2 m from a horizontal attitude and commanding a desired pitch angle of 45°. We chose a tail tip mass that allowed sufficient body rotation within the available range of tail motion ($\pm 100^\circ$). We chose controller gains such that the manoeuvre could be completed in less than 150 ms without body angle oscillation (outside the range of tail motion). Proportional feedback control alone was unable to control overshoot and we thus used only PD feedback control in the final trials.

We drove the robot off an inclined 'ski-jump' ramp. The ramp declined at 20° to the horizontal for 150 cm and inclined at the same angle for the final 25 cm. The robot accelerated to 2.5 m s⁻¹ before becoming airborne. When the front wheels of the robot left the ramp, the unbalanced gravitational moment imparted an angular momentum perturbation. We repeated trials nine times each for the active and passive cases. The magnitude of the perturbation depended on the duration of unbalanced moment and, hence, on the speed of the vehicle as it left the ramp.

Velociraptor model. To model the tail stabilization performance of an extinct theropod dinosaur, we estimated mass properties from a two-dimensional reconstruction. Although some mass and MOI data were available from a previous model²⁵, separate trunk and tail estimates were not. We represented the head and trunk as ellipsoids, the neck as an elliptical cylinder and the tail as a truncated cone by digitizing points on the dorsal and sagittal views of the reconstruction. To be conservative in our estimate of tail effectiveness, the cone accounted for the envelope of the vertebrae, without additional external musculature. The density of body tissue was set to 1,000 kg m⁻³, whereas tail density was set higher (1,500 kg m⁻³) to account for the high proportion of bone (the density of which is typically set to 2,000 kg m⁻³). We then scaled limb masses following ref. 25, oriented them as in the reconstruction and calculated their contribution to the body MOI. Our combined trunk–tail MOI agreed well with that of ref. 25. We modelled the animal in two configurations—one in which the limbs were extended and one in which the limbs were held against the body or retracted—and used the average of the two for the effectiveness estimate. We added 15% to the body MOI and subtracted 15% from the tail MOI to generate the lower bound of effectiveness in Fig. 3; the converse procedure generated the upper bound.

26. Dowling, J. J. *et al.* The uncertainty of the pendulum method for the determination of the moment of inertia. *Med. Eng. Phys.* **28**, 837–841 (2006).